Drift waves and ion temperature gradient instabilities in the large linear device SPEKTRE

E. Gravier ✉ ; F. Brochard ; M. Lesur ; J. Moritz ; S. Heuraux ; D. Genève; T. Rouyer ;
D. Del Sarto ; E. Faudot ; A. Ghizzo ; N. Lemoine ; T. Réveillé ; G. Urbanczyk

Check for updates

View Online   Export Citation

Articles You May Be Interested In

Global ICRH modeling in large noncircular tokamak plasmas with finite temperature

AIP Conference Proceedings (September 1987)

ICRH coupling optimization and impurity behavior in EAST and WEST

AIP Conf. Proc. (September 2020)

ICRH of JET and LHD Majority Ions at Their Fundamental Cyclotron Frequency

AIP Conference Proceedings (September 2007)

AIP Publishing

Physics of Plasmas

Special Topics Open for Submissions

Learn More

AIP Publishing

Drift waves and ion temperature gradient instabilities in the large linear device SPEKTRE

View Online   Export Citation   CrossMark

E. Gravier,[a] 🔟 F. Brochard, 🔟 M. Lesur, 🔟 J. Moritz, 🔟 S. Heuraux, 🔟 D. Genève, T. Rouyer, D. Del Sarto, 🔟
E. Faudot, 🔟 A. Ghizzo, 🔟 N. Lemoine, 🔟 T. Réveillé, 🔟 and G. Urbanczyk 🔟

AFFILIATIONS

Université de Lorraine, CNRS, Institut Jean Lamour, UMR 7198, F-54000 Nancy, France

[a]Author to whom correspondence should be addressed: etienne.gravier@univ-lorraine.fr

ABSTRACT

The objective of this work is to linearly investigate the plasma instabilities that will be observed in the linear SPEKTRE device, currently being assembled at Institut Jean Lamour. Two configurations are considered. In the first configuration, the magnetic field is set to 0.1 T with no ion temperature gradient (ITG), resulting in the observation of only collisional drift waves (DW). In the second configuration, the magnetic field is set to 0.44 T, and ions can be heated using an ion cyclotron radiofrequency heating (ICRH) system to establish an ITG. Under these conditions, two major types of instabilities may be observed: collisional DW and ITG instabilities. ITG instabilities become more unstable than DW when the ratio of the characteristic lengths of the ion temperature to ion density profiles $\eta = \Omega_T^* / \Omega_n^* > 2.6$. The observation of such a transition between the two types of instabilities will be possible on this machine using the ICRH system. The azimuthal mode number m of the most unstable mode is significantly larger for helium plasma compared to argon plasma. Furthermore, for the plasma parameters considered in both configurations, a fluid model is often sufficient to accurately describe DW, while a kinetic model is required to accurately describe ITG instabilities. There is a 30% difference between the ITG instability growth rates predicted by the fluid model and those predicted by the kinetic model.

I. INTRODUCTION

Sheaths, Plasma Edge, Kinetic Turbulence Radiofrequency Experiment (SPEKTRE) is a research platform in plasma physics and nuclear fusion currently under construction at the Institut Jean Lamour in Nancy.[1] It will produce a plasma 40 cm in diameter and 5.9 m in length, under a magnetic field of 0.44 Tesla. According to the ion heating system, higher values can be achieved later if needed, but this requires an updated current generator. The topics to be investigated include the physics of radio-frequency sheaths and ion cyclotron radiofrequency heating (ICRH), instabilities and turbulent transport in magnetized plasmas, targeted studies on plasma–wall interactions (including liquid metal walls), and surface treatments by magnetized plasmas.

One of the main objectives will be to perform fundamental investigations of selected plasma instabilities in large, magnetized plasma columns, which exhibit characteristics similar to those of edge plasmas in tokamaks with open magnetic field lines. The plasma edge, which evolves in the Scrape-Off Layer (SOL), follows magnetic field lines that are open and connected to the machine's divertor. This design aims to distance the plasma–wall interaction from the confined core plasma. In this region, the plasma is significantly less dense and cooler than in the core plasma, where the magnetic surfaces are closed. The boundary between these two regions is called the separatrix, which is the last closed flux surface. The transition between these regions is quite abrupt and plays a major role in plasma confinement. The region close to the separatrix can exhibit specific instabilities and turbulence that can be reproduced in SPEKTRE. These instabilities and plasma turbulence are sensitive to the presence of neutral particles in this region, originating from plasma–wall interactions or voluntary injection. The aim here is to characterize the physics of instabilities that can be caused by interactions of charged particles with neutrals. For example, when electrons collide with neutrals, collisional drift waves (DW) become destabilized and can be observed.

Here, we focus on two potential instabilities that may occur in the SPEKTRE device: collisional DW and ion temperature gradient (ITG) instabilities. The goal is to predict the mode numbers that will develop as well as the specific characteristics of the instabilities that will be observed. These instabilities are driven by gradients in the density or

temperature of ions and electrons. Low-frequency fluctuations are observed in tokamak plasmas as well as in cylindrical magnetized plasma columns,[2–17] this is why these cylindrical machines are of fundamental interest and provide a testing ground for comparing numerical simulations with experiments.

DW in MIRABELLE[9] and ITG in Columbia Linear Machine (CLM)[10] have been observed. In MIRABELLE, however, Kelvin–Helmholtz (KH) instabilities were observed by incorporating a limiter[9,11] that restricted the diameter of the plasma column ("top-hat-like" source profile), creating a radial electric field capable of triggering KH instabilities (flute instabilities with $k_{\parallel} = 0$) at low magnetic field.[9] Without this limiter and for strong magnetic field, only DW with $k_{\parallel}$ different from zero were observed. In CLM, ITG instabilities were detected in the presence of an ion temperature gradient.[10] In LAPD, it has been shown that KH instabilities are primary contributors to heat and particle transport across the magnetic field.[18] In this paper, we limited our investigation to DW and ITG instabilities. However, in the future, we plan to study Kelvin–Helmholtz (KH) and Poloidal Velocity Gradient (PVG) instabilities by identifying methods to trigger them in the SPEKTRE device. This could involve implementing an ExB drift in the azimuthal direction (for KH instabilities, by applying a radial electric field) or introducing shear in the parallel ion velocity (for PVG, by setting $dv_{\parallel}/dr$ to be nonzero).

Numerical simulations play a crucial role in advancing our understanding of plasma instabilities. For instance solving three-dimensional fluid equations is the most effective way to compute the plasma response to perturbed electromagnetic fields, especially when wave–particle interactions are outside the working conditions and when collisions are predominant.[18] However, predicting turbulent transport in nearly collisionless fusion plasmas often necessitates solving gyrokinetic equations.[17,19] The theoretical and numerical studies detailed in this paper are based on either a two-fluid model or a kinetic water-bag model.[7,8,20] The water-bag approach simplifies the full kinetic equation into a set of hydrodynamic equations while retaining most of its kinetic characteristics. When compared to the models used in Refs. 17 and 19, the equilibrium electric potential shear near the boundaries is not taken into account in our water-bag approach, but finite parallel wave-numbers are considered. Furthermore, in this paper, the plasma is only partially ionized, with electron-neutral collisions playing a major role, whereas in Refs. 17 and 19, the plasma is fully ionized, and Coulomb collisions are considered.

The relevance of the SPEKTRE experiments and of this study is based on existing experimental works realized in similar conditions but with smaller plasma diameters in the CLM.[13,14] CLM is a linear device that utilizes radio frequency (RF) heating to heat the core of the plasma column and generate a peaked ion temperature profile. A hydrogen plasma was generated in CLM, where an ITG mode m = 2 mode was observed. We have already compared the experimental results from CLM[14] with our theoretical Water-Bag model of the ITG instability.[7] The results have shown to be in fairly good agreement with the predictions of the water-bag model. This provides confidence in using this model to predict the instabilities and modes that will be observed in the SPEKTRE device, though higher modes are anticipated. Hence, we investigate these high modes expected with SPEKTRE plasma parameters, assuming Gaussian equilibrium profiles for density and temperature. Two gases are under consideration in the present work: argon and helium.

SPEKTRE and LAPD[15] are both large linear plasma devices designed to study magnetized plasmas under controlled magnetic fields, which make them suitable for studying long-wavelength instabilities and electrostatic turbulence. LAPD is a larger device, with plasma length $L \simeq 18$ m and plasma diameter $D \simeq 56$ cm (compared to $L \simeq 6$ m and $r \simeq 20$ cm for SPEKTRE) and the plasma sources are different (hot cathode vs helicon), but these differences are expected to have only a minor impact on the dynamic instability regimes produced in the two devices. However, SPEKTRE's focus on higher magnetic fields (0.44 vs 0.25 T) and ICRF heating, with a heating capability of 100 kW, are expected to result in higher confinement and potentially more energetic modes compared to LAPD, with changes in frequency and growth rate depending on the strength of the magnetic field. The ion temperature gradient will be much more pronounced in SPEKTRE, which is fundamental to the study of ITG instabilities.

The paper is structured as follows: Sec. II introduces the linear device SPEKTRE and its characteristics, along with the two configurations under investigation in this study. Section III outlines the fluid model for electrons and the kinetic model for ions, along with their assumptions and limitations. Section IV presents a comparison between global and local approximation models. Section V examines the case of argon and helium plasmas. Finally, Sec. VI emphasizes the significance of a kinetic model to accurately describe ITG instabilities. A comparison of the modes predicted by the kinetic model with those obtained from the fluid model is presented.

II. THE LINEAR DEVICE SPEKTRE

SPEKTRE is a new magnetized plasma research facility, depicted in Fig. 1, about to begin operation. In the initial operational phase (referred to hereafter as case 1 with $B = 0.1$ T, see Table I), the machine will undergo progressive upgrades. Once these upgrades are complete, SPEKTRE will possess several unique features: a large plasma volume, a strongly magnetized plasma column, meaning that fluctuations occur on time scales much longer than particle gyromotion, and the ion Larmor radius is much smaller than the characteristic length scale of density gradient, with 100 kW of ICRF heating, and numerous diagnostic capabilities, including fast visible cameras, probe arrays, spatially resolved optical emission spectroscopy, interferometer, and reflectometer. These characteristics will make it an accessible instrument for studying a wide range of phenomena in magnetized plasmas.[1] This configuration will be referred to hereafter as case 2 with $B = 0.44$ T (see Table I).

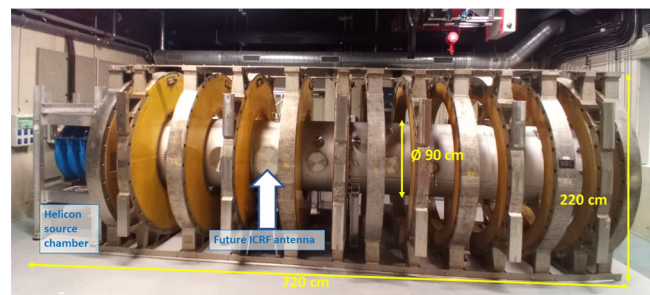For both cases density and temperature profiles will be assumed to be Gaussian:

FIG. 1. Photograph of the SPEKTRE machine during the final assembly phase.

TABLE I. The main parameter values for both configurations (cases 1 and 2) are as follows: B is the magnetic field, T_e and T_i the electron and ion temperatures, a the radius of the cylindrical plasma, L the length of the cylinder, r_N and r_T are characteristic lengths of the density and temperature profiles, $k_{\parallel}$ is the wavenumber along the parallel direction, ν_e the electron-neutral collision rate and u_0 the electron velocity along the axis of the cylinder. In SPEKTRE, according to the helicon plasma source, the plasma density will be equal or greater than 10^{16} m^{-3}, the neutral density equal or greater than 10^{19} m^{-3}.

	B (T)	T_{e_0} (eV)	T_{i_0} (eV)	a (m)	L (m)	$r_{N_{e,i}}$ (m)	r_{T_e} (m)	r_{T_i} (m)	$k_{\parallel}$ (m^{-1})	ν_e (s^{-1})	u_0 (v_{T_e})
Case 1	0.1	3.0	0.03	0.2	5.9	0.2	$+\infty$	$+\infty$	1.065	5.0×10^5	0.3
Case 2	0.44	10.0	10.0	0.2	5.9	0.2	$+\infty$	0.0894	1.065	5.0×10^5	0.3

$$n(r) = n_0 \exp(-r^2/r_N^2), \tag{1}$$

$$T(r) = T_0 \exp(-r^2/r_T^2), \tag{2}$$

with r_N and r_T the characteristic lengths of the density and temperature profiles. The density profile will be the same for ions and electrons, while the temperature profiles may vary depending on the specific case considered (see Table I). One has $\kappa_n = \frac{1}{n}\partial_r n = -2r/r_N^2$ and $\kappa_T = \frac{1}{T}\partial_r T = -2r/r_T^2$ so that the ratio $\eta = \Omega_T^*/\Omega_n^* = \kappa_T/\kappa_N = r_N^2/r_T^2$ is constant over the radius. It should be noted that the knowledge of exact experimental profiles is necessary to accurately predict the most unstable modes. In this work, since we do not know exactly the future profiles that will be obtained in SPEKTRE, we choose the profiles from Fig. 2, which allow us to identify trends between the two different magnetic configurations and between the two different gases. Even if the most unstable mode may vary slightly depending on the profiles, the trends will remain the same, as will the orders of magnitude of the obtained frequencies. The advantage of the profiles defined in Fig. 2 is that they are not too affected by the local nature of the gradients: the value of η and the electron diamagnetic frequency do not depend on r.

As often observed in linear devices, the parallel mode number is equal to 1 ($k_{\parallel} = \pi/L$ in MIRABELLE and CLM[9–11]) or 2 ($k_{\parallel} = 2\pi/L$ in VINETA[12]). For this study the parallel wavenumber is set to $2\pi/L$, where L is the length of the cylinder.

For the first configuration, the magnetic field will be set to 0.1 T (see case 1 in Table I). The electron temperature will be approximately 3 eV, and the ions will remain at the same temperature as the neutrals. In this configuration, no heating process for the charged particles is planned; therefore, ion and electron temperatures are assumed to be constant [see Fig. 2(b)].

For the second configuration the magnetic field will be set to 0.44 T (see case 2 in Table I). The electron temperature will be approximately 10 eV, and the ions will be heated using an ICRH, resulting in a nonzero ITG [see Fig. 2(b)]. In SPEKTRE conditions, the absorption should be proportional to the density profile which results from the ionization process induced by the electric field distribution of the launched wave, assumed to have a poloidal invariance in average as observed in IShTAR.[21]

III. MODELING OF COLLISIONAL DRIFT WAVES (DW) AND ION TEMPERATURE GRADIENT (ITG) INSTABILITIES

A. Generalities

We consider a cylindrical plasma of radius a, confined by a uniform magnetic field $\mathbf{B} = B\mathbf{u}_z$, where $\mathbf{u}_z$ is the unit vector along the cylinder axis. Three species are considered: the neutral gas, the electron fluid, which is free to collide and exchange momentum with the neutral gas, and finally, the ion fluid. A helicon plasma source using a RF

wave will be employed in SPEKTRE. The plasma density will vary as a function of the input power and the magnetic field near the antenna, as described by Ref. 22. At low input power, the plasma density will be on the order of 10^{16} m^{-3}, typical of Capacitively Coupled Plasma (CCP) mode. Higher plasma densities will be achieved with increased power, transitioning first to Inductively Coupled Plasma (ICP) mode, and then, to Helicon Wave (HW) mode. Initially, we will focus on plasma densities around 10^{16} m^{-3}, with an ionization rate of 10^{-3}.

For this plasma density, and assuming an electron temperature of 10 eV, the electron-neutral collision rate is approximately 5×10^5 s^{-1}[23] the ion-neutral collision rate is about 10^4 s^{-1}[24] and the electron-ion Coulomb collision rate is roughly 5×10^4 s^{-1}. These values are
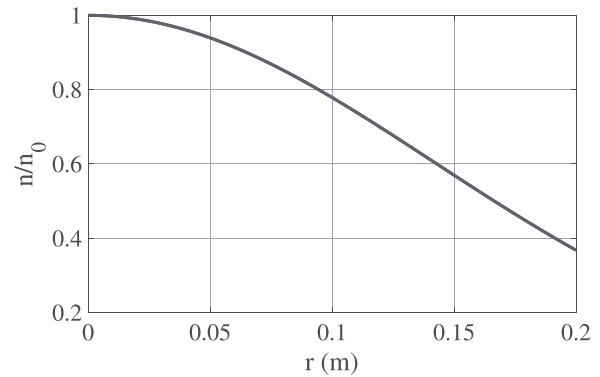
(a) Density profile.
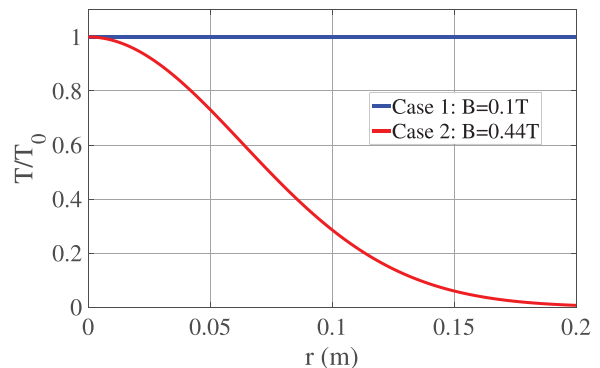
(b) Ion temperature profile (case 1 in blue and case 2 in red).

FIG. 2. Density (same for both cases) and ion temperature profiles. (a) Density profile. (b) Ion temperature profile (case 1 in blue and case 2 in red).

around similar for both argon and helium. Therefore, in this study and to get trends, we will focus on electron-neutral collisions and treat them as constant. For higher plasma densities, Coulomb collisions may become more significant, increasing plasma resistivity and enhancing the resistive behavior of DW, making DW more unstable than ITG modes. The helicon source of the SPEKTRE device, based on its available power,[1] should enable us to explore various regimes, from CCP to ICP and HW. However, we will begin by operating in the CCP and/or ICP regimes.

Additionally, it is assumed that fluctuations in the magnetic field are negligible. The ion and electron populations are coupled by the quasi-neutrality equation.

We assume that all instability and collision frequencies are small when compared to the ion cyclotron frequency $\Omega_c = eB/m_i$, ions are assumed ionized once, with e the absolute value of the electron charge and m_i the ion mass. At maximum, the ratio observed hereafter with the real frequencies predicted in Sec. V will be 1/25 for $B = 0.1$ T and for an argon plasma. Moreover, at maximum, the ratio ρ_i/a, with ρ_i the ion Larmor radius, is 0.02 in case 2 and for an argon plasma.

Furthermore, the electron thermal velocity is consistently much greater than the phase velocity of the instabilities, and given the inclusion of electron-neutral collisions, employing a fluid model for electrons is warranted. However, for ions, the ion thermal velocity is often of the same order of magnitude as the phase velocity, facilitating strong wave–particle interactions that requires the use of a kinetic model to describe the ion population behavior.

Here, key elements of the model used are given, and more details can be found in Ref. 7.

B. Electrons

The approach taken here assumes that the phase velocity of the instabilities is much lower than the electron thermal velocity. Additionally, electron-neutral collisions are considered. As a result, we assume kinetic effects to be negligible, meaning the electron distribution function remains close to Maxwellian. This allows us to employ a fluid model with isothermal compression to close the system of equations. A viscosity term is introduced into the fluid equation of motion to account for electron-neutral collisions.

The electron model equations consist of the fluid equations for a weakly ionized plasma as provided by Self[25] or Ellis et al.[26,27] Collisions with neutrals dominate and are characterized by the collision frequency ν_e. The fundamental density profile $n(r)$ is assumed to solely depend on the radial coordinate r. The presence of a radial density gradient induces an azimuthal electron diamagnetic drift that writes:

$$\mathbf{v}_d = -\frac{T_e}{eB}\kappa_n \mathbf{u}_\theta, \qquad (3)$$

with T_e the electron temperature. This drift serves as a source of free energy that can contribute to the growth of fluctuations. Furthermore, we adopt the assumption, as in Refs. 26 and 27, that in the equilibrium state, electrons drift parallel to the magnetic field at a speed u_0.

In the following, the results come from a linear analysis with small perturbations and assuming an electrostatic potential of the form:

$$\Phi(r, \theta, z, t) = \phi(r) \exp[i(m\theta + k_\parallel z - \omega t)] + c.c., \qquad (4)$$

and for the electron density:

$$n_e(r, \theta, z, t) = \tilde{n}_e(r) \exp[i(m\theta + k_\parallel z - \omega t)] + c.c., \qquad (5)$$

with m the azimuthal mode, $k_\parallel$ the parallel wavenumber and $\omega = \omega_r + i\omega_i$ the angular frequency.

Linearizing the electron fluid model and following Self[25] or Ellis et al.,[26,27] yields a set of coupled equations, e.g., Eqs. (4), (6), and (7) of Ref. 27. Note that in the Eq. (7) of Ref. 27 a term $-e\tilde{n}B(\mathbf{v}_d \times \hat{z})$ in the right-hand side is missing. The relationship between the perturbed electron density $\tilde{n}_e$, having the same dependencies as in Eq. (4), and the pertubed electrostatic potential ϕ, is expressed as follows:

$$\tilde{n}_e = n \frac{\omega^\star + i\nu_\parallel}{\omega - k_\parallel u_0 + i\nu_\parallel} \frac{e\phi}{T_e}, \qquad (6)$$

with $\omega^\star = -k_\theta \frac{T_e}{eB}\kappa_n$, $k_\theta = m/r$, $\nu_\parallel = \frac{k_\parallel^2 T_e}{m_e \nu_e}$. With our parameters, the ratio $\frac{a}{L_n} \simeq \frac{a}{r_n} \simeq 1$, the electron diamagnetic frequency $\omega^\star$ is of the order of 10^4 s^{-1}, and $\nu_\parallel$ of the order of 10^6 s^{-1}.

C. Ions

When the ion thermal velocity v_{Ti} approaches the phase velocity $v_\varphi = \omega/k_\parallel$, with ω the wave angular frequency and $k_\parallel$ its parallel wavenumber, resonant interactions between waves and particles become crucial in determining the instability growth rate. Furthermore, ion-neutral collisions are disregarded hereafter. Hence, a kinetic model providing the distribution function is necessary. The kinetic and fluid descriptions of the ITG instability can result in different instability thresholds and linear growth rates. Additionally, fluid models are often reported to overestimate the level of turbulent transport.[28]

We assume that fluctuations have time scales much greater than the cyclotron period of charged particles: $\omega \ll \Omega_c$ with ω the instability frequency. Moreover, the ion Larmor radius is much smaller than the density gradient characteristic length $n/|\nabla n|$.

This gyrokinetic ordering[29] facilitates the separation between fast gyromotion and slow dynamics perpendicular to the magnetic field direction. The gyrokinetic model fully utilizes μ-invariance to eliminate perpendicular kinetic variables in the Vlasov equation, where $\mu = m_i v_\perp^2/2B$ represents the first adiabatic invariant, associated with perpendicular dynamics. Consequently, the phase space reduces to four dimensions: three in real space and one in velocity space. For a given value of μ, the ions are characterized by the statistical distribution function $f(\mathbf{r}, v_\parallel, t)$ of their guiding-center (GC) position. The variable $v_\parallel$ denotes the velocity parallel to the magnetic field direction. The gyrokinetic Vlasov equation is as follows:

$$\partial_t f + \left(\frac{\mathbf{E} \times \mathbf{B}}{B^2} + v_\parallel \mathbf{u}_z\right) \cdot \nabla f + \dot{v}_\parallel \partial_{v_\parallel} f = 0, \qquad (7)$$

with $\dot{v}_\parallel = qE_\parallel/m_i$, q the ionic charge, $\mathbf{E} = -\nabla J_0 \Phi$, Φ the electric potential, $J_0(k_\perp v_\perp/\Omega_c)$ the gyroaverage operator, $k_\perp$ the perpendicular wave number, $v_\perp \simeq v_{T_i} = \sqrt{T_i/m_i}$, T_i the ion temperature and m_i the ion mass. The thermal velocity is kept constant, but the operator J_0 depends on m the azimuthal mode number ($k_\theta = m/r$), ensuring that Finite Larmor Radius effects are properly accounted for and play a significant role in stabilizing high poloidal wave-numbers.

Here, μ, or the perpendicular velocity $v_\perp$, serves as a parameter defining distinct particle classes, each with a unique Larmor radius ($r_{L_i} = v_\perp/\Omega_c$). When averaging the Larmor radius over a Maxwellian distribution function, the operator J_0 can be approximated by an

exponential function of the thermal velocity and the cyclotron frequency. It is worth noting that electrons are assumed to move with a zero Larmor radius, aligning the electron density with the guiding-center density, as the Larmor radius for electrons is much smaller compared to ions.

The water-bag (WB) concept uses Liouville's invariance to further reduce the dimension of phase space. A comprehensive explanation of the Gyro-Water-Bag model and the procedure for selecting water-bag parameters can be found in Refs. 7 and 20.

An ion distribution function is chosen:

$$f_{MWB}(\mathbf{r}, v_{\parallel}, t) = \sum_{j=1}^{M} A_j \left\{ H\left[v_{\parallel} - v_j^-(\mathbf{r}, t) \right] - H\left[v_{\parallel} - v_j^+(\mathbf{r}, t) \right] \right\}, \tag{8}$$

with M the number of bags, H the Heaviside step-function. The interesting property of the WB distribution is the absolute time invariance of the bag heights A_j. Consequently, the evolution of the system is determined by the evolution of the contours $v_j^+(\mathbf{r}, t)$ and $v_j^-(\mathbf{r}, t)$.

Introducing this distribution function in the gyrokinetic equation leads to the following set of equations, called contour equations:[20]

$$\partial_t v_j^{\pm} + \frac{\mathbf{E} \times \mathbf{B}}{B^2} \cdot \nabla_{\perp} v_j^{\pm} + v_j^{\pm} \nabla_{\parallel} v_j^{\pm} = \dot{v}_j^{\pm} = \frac{qE_{\parallel}}{m_i}. \tag{9}$$

In the framework of linear analysis, the velocities write:

$$v_j^{\pm} = \pm a_j(r) + W_j^{\pm}(r) \exp[i(m\theta + k_{\parallel} z - \omega t)] + c.c., \tag{10}$$

with a_j the velocity of the jth bag at equilibrium, i.e., $v_j^+ = a_j$ and $v_j^- = -a_j$ at equilibrium, for symmetric bags in the velocity coordinate.

The ion polarization drift can be explicitly introduced in the Vlasov equation or equivalently through a perturbed ion density,[7] so that the total perturbed ion density reads:

$$\tilde{n}_{i_{tot}} = J_0 \tilde{n}_i + \nabla_{\perp} \cdot \left(\frac{n_0}{\Omega_c B} \nabla_{\perp} \phi \right), \tag{11}$$

with

$$\tilde{n}_i = \sum_{j=1}^{M} A_j \left(W_j^+ - W_j^- \right). \tag{12}$$

Hereafter, we assume ions with one positive charge $q = e$.

Following the same procedure as in Refs. 7 and 20, one obtains:

$$\tilde{n}_{i_{tot}} = \frac{nq}{T_i} J_0^2 \phi \sum_{j=1}^{M} \alpha_j \frac{k_{\parallel}^2 v_{T_i}^2 - \omega \Omega_j^{\star}}{\omega^2 - k_{\parallel}^2 a_j^2}$$
$$+ \frac{n}{\Omega_c B} \left[\frac{d^2\phi}{dr^2} + \left(\kappa_n + \frac{1}{r} \right) \frac{d\phi}{dr} - k_{\theta}^2 \phi \right], \tag{13}$$

with $\Omega_j^{\star} = k_{\theta} \frac{T_i}{qB} \kappa_j$, $\kappa_j = \frac{1}{a_j} \partial_r a_j$, $\alpha_j = \frac{2a_j A_j}{n}$.

Finite Larmor Radius effects are contained in the gyroaveraged distribution function and in the second term of the right-hand side of Eq. (13), commonly known as the polarization effect. From a physical perspective, numerous interesting results can be achieved even with small values of M, kinetic effects are accurately captured with just 10 bags.[20] Hereafter, the bag number M will be chosen equal to 15, high enough to make sure that the kinetic real frequencies and instability

growth rates converge. Additionally and even if it is not used here, it is worth noting that the water-bag approach is not limited to Maxwellian distribution functions: it enables the consideration of any arbitrary function of the parallel velocity $v_{\parallel}$.

D. Dispersion relation - Kinetic model

These contours of the ion water-bag model and electrons are coupled by the quasi-neutrality equation:

$$\tilde{n}_{i_{tot}} = \tilde{n}_e. \tag{14}$$

After some algebra, one can express all perturbation fields in terms of the potential $\phi(r)$, and obtain a differential equation for $\phi(r)$. Using Eqs. (6) and (13), the dispersion relation writes:

$$\frac{d^2\phi}{dr^2} + \left(\kappa_n + \frac{1}{r} \right) \frac{d\phi}{dr} + [Q(r) - k_{\theta}^2]\phi = 0, \tag{15}$$

with, noting $\tau = \frac{T_i}{T_e}$:

$$Q(r) = \frac{J_0^2}{r_{Li}^2} \left(\sum_{j=1}^{M} \alpha_j \frac{k_{\parallel}^2 v_{T_i}^2 - \omega \Omega_j^{\star}}{\omega^2 - k_{\parallel}^2 a_j^2} \right) - \frac{\tau}{r_{Li}^2} \left(\frac{\omega^{\star} + i\nu_{\parallel}}{\omega - k_{\parallel} u_0 + i\nu_{\parallel}} \right). \tag{16}$$

The Eq. (15) can also be written:

$$L\phi = -Q(r)\,\phi, \tag{17}$$

with

$$L\phi = \frac{d^2\phi}{dr^2} + \left(\frac{1}{r} + \kappa_n \right) \frac{d\phi}{dr} - \frac{m^2}{r^2} \phi. \tag{18}$$

It has to be solved with the boundary condition:

$$\phi(a) = 0, \tag{19}$$

that expresses the isopotential nature of the vacuum vessel, with a the radius of the cylindrical plasma.

E. Dispersion relation - Fluid model

To compare the outcomes provided by a kinetic model with those given by a fluid model, it is feasible to compute the moments of Eq. (7) and derive a fluid model for ions. To derive the dispersion relation, the third moment is used, assuming the heat flux is zero. The linearization procedure remains unchanged, as does the polarization term we consider. In that fluid approach, $Q(r)$ writes:

$$Q(r) = \frac{J_0^2}{r_{Li}^2} \frac{k_{\parallel}^2 v_{T_i}^2 \left(1 + \frac{2\Omega_n^{\star} - \Omega_T^{\star}}{\omega} \right) - \omega \Omega_n^{\star}}{\omega^2 - 3k_{\parallel}^2 v_{T_i}^2} - \frac{\tau}{r_{Li}^2} \left(\frac{\omega^{\star} + i\nu_{\parallel}}{\omega - k_{\parallel} u_0 + i\nu_{\parallel}} \right), \tag{20}$$

with $\Omega_n^{\star} = k_{\theta} \frac{T_i}{qB} \kappa_n$ and $\Omega_T^{\star} = k_{\theta} \frac{T_i}{qB} \kappa_T$.

F. Local approximation

Here, we assume that $d/dr = 0$ (local approximation, assuming that the amplitude of the perturbations remains constant throughout the radial domain), then $k_{\perp} = k_{\theta} = m/r$ ($k_r = 0$) and the dispersion

relation [Eq. (17)] writes $Q(r) = k_\theta^2 = m^2/r^2$, or, in the case of the kinetic model:

$$\frac{J_0^2}{r_{Li}^2}\left(\sum_{j=1}^{M}\alpha_j\frac{k_\parallel^2 v_{Ti}^2 - \omega\Omega_j^\star}{\omega^2 - k_\parallel^2 a_j^2}\right) - \frac{\tau}{r_{Li}^2}\left(\frac{\omega^\star + i\nu_\parallel}{\omega - k_\parallel u_0 + i\nu_\parallel}\right) = k_\theta^2, \quad (21)$$

and in the case of fluid model:

$$\begin{aligned}
&\delta\omega^4 + [(\tau + \delta)i\nu_\parallel - \delta\omega_\parallel + \Omega_n^*(J_0^2 - 1)]\omega^3\\
&+ [i\nu_\parallel J_0^2\Omega_n^* - J_0^2(\omega_\parallel\Omega_n^* + \Omega_\parallel^2) - 3\Omega_\parallel^2\delta]\omega^2\\
&+ \left[3\Omega_\parallel^2\Omega_n^* + J_0^2\Omega_\parallel^2(\Omega_T^* - 2\Omega_n^*) + \omega_\parallel\Omega_\parallel^2(J_0^2 + 3\delta)\right.\\
&\left.- i\nu_\parallel\Omega_\parallel^2[3(\tau + \delta) + J_0^2]\right]\omega\\
&+ J_0^2\Omega_\parallel^2(\omega_\parallel - i\nu_\parallel)(2\Omega_n^* - \Omega_T^*) = 0,
\end{aligned} \quad (22)$$

with $\omega_\parallel = k_\parallel u_0$, $\Omega_\parallel = k_\parallel v_{Ti}$, and:

$$\delta = k_\theta^2 r_{Li}^2. \quad (23)$$

G. Global modes

Now, we consider that the density profile depends on r (global modes, or radially distributed modes): the radial derivative d/dr is no longer neglected.

As the density profile is assumed to be Gaussian,

$$n(r) = n_0 \exp(-r^2/r_N^2), \quad (24)$$

the electron diamagnetic frequency $\omega^\star = -k_\theta\frac{T_e}{eB}\kappa_n$ is independent of r.

By setting $S = Qa^2$ and $\alpha = r/a$, the differential Eq. (15) can be written:

$$\frac{d^2\phi}{d\alpha^2} + \left(\frac{1}{\alpha} - 2\alpha\frac{a^2}{r_N^2}\right)\frac{d\phi}{d\alpha} + \left[S - \frac{m^2}{\alpha^2}\right]\phi = 0. \quad (25)$$

Or:

$$L\phi = -S(r)\phi, \quad (26)$$

with

$$L\phi = \frac{d^2\phi}{d\alpha^2} + \left(\frac{1}{\alpha} - 2\alpha\frac{a^2}{r_N^2}\right)\frac{d\phi}{d\alpha} - \frac{m^2}{\alpha^2}\phi. \quad (27)$$

Arbitrarily, we also choose the gyro-average operator to be independent of r (or α). It is written as $J_0^2 = \exp(-k_\theta^2 r_{Li}^2)$, with r_{peak} an arbitrary choice of r for the estimation of $k_\theta = m/r$. r_{peak} denotes the localization of the maximum perturbation as provided by the global model when S does not depend on r. This arbitrary choice is made only for the evaluation of J_0, which is a correction operator that takes into account the effects of the finite Larmor radius. Another choice would only slightly alter the determination of the most unstable mode and the trends would remain the same.

Therefore, in case 1 we observe that S does not depend on r: the dispersion relation and S can be solved using a change of variables and a hypergeometric function, as shown in Ref. 30, or by employing a shooting method.[25–27] For case 2, S depends on r and the dispersion relation can be solved using a spectral method.[7,31,32]
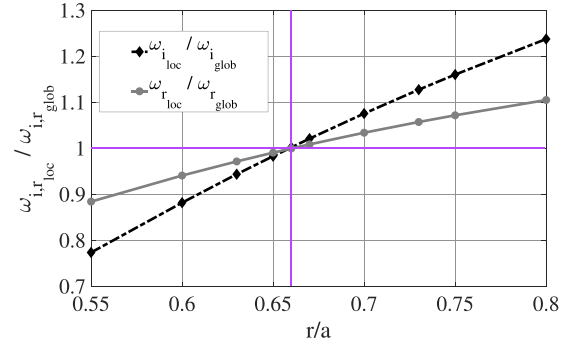

FIG. 3. Ratio of local vs global instability growth rates and real frequencies plotted against r, the chosen localization for the calculation of $k_\theta = m/r$ in the case of the local approximation model. The plasma parameters are $\eta = 0$, $B = 0.1$ T, $T_e = 3$ eV, $T_i = 0.03$ eV, in an argon plasma, and $m = 8$ is identified as the most unstable mode (DW instability). A good agreement is observed when r for the local approximation model equals r_{peak}, which denotes the localization of the maximum perturbation as provided by the global model.

IV. GLOBAL VS LOCAL APPROXIMATION MODELS

In this section, we explore the significance of considering global modes vs local-approximation modes. We focus on first case ($B = 0.1$ T), considering an argon plasma with $\eta = 0$. The most unstable mode predicted by the kinetic global model [Eqs. (15) and (16)] is $m = 8$, corresponding to a DW instability. We compare these results with those obtained from the local kinetic model [Eq. (21)].

The results are depicted in Fig. 3. The ratio of local over global instability growth rates and real frequencies are plotted against r, representing the localization chosen for the calculation of $k_\theta = m/r$ in the case of the local approximation model. In this local approximation model, a value of r is required for the estimation of k_θ. A good agreement is observed when r for the local approximation model is set to equal to r_{peak}, here, $r = 0.66a$, where r_{peak} represents the localization of the maximum of the perturbation as provided by the global model. If real frequencies show little sensitivity to the choice of r, the instability growth rate is more influenced by it, along with the predicted most unstable mode. Nevertheless, if the mode's localization is approximately known, the local dispersion relation is sufficient for estimating the instability growth rates.

To illustrate the capability of the global model in predicting the 3D structure of the instabilities, we show in Fig. 4 the 3D structure of the plasma potential corresponding to the most unstable mode predicted by the global kinetic model (case 1, $B = 0.1$ T, $m = 8$, DW instability). The localization of the azimuthal mode $m = 8$ is observed in a cross section of the cylinder, along with the parallel mode along the axis of the cylinder.

Hereafter, the local model will be used to investigate the competition between DW and ITG. As already mentioned, the profiles from Fig. 2 allow us to identify trends between the two different magnetic configurations and between the two different gases, and their advantage is that they are not too affected by the local nature of the gradients.

V. CASES OF ARGON AND HELIUM

We use the global kinetic water-bag dispersion relation [Eq. (21)] to investigate the possibility of observing collisional DW or/and ITG instabilities in the plasma column. Two cases (see Table I) are
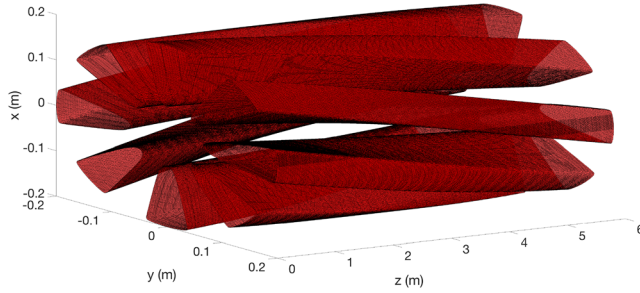
FIG. 4. View of the 3D plasma potential most unstable mode ($m = 8$, DW instability). The plasma parameters are $B = 0.1$ T, $T_e = 3$ eV, $T_i = 0.03$ eV, in an argon plasma. The magnetic field is oriented along the z-axis, and its intensity is uniform to more than 96% within the plasma volume. Here, the boundaries of the structures are delineated by iso-gradients of the plasma potential.

considered. Here, the parallel wavelength is taken to be constant and equal to the length of the device.

For the first case with $B = 0.1$ T, temperature profiles are flat, so only DW can be observed. The real frequency ω_r and the instability growth rate ω_i are plotted against the azimuthal number m (Fig. 5). For argon, the most unstable mode is characterized by the highest instability growth rate ($m = 8$), with a real frequency of 8.87×10^3 s^{-1}. This positive real frequency indicates that the wave propagates in the direction of the electron diamagnetic velocity, in agreement with [Eq. (3)], and as expected for collisional DW. Moreover, we observe that ω_r is of the order of magnitude of $\omega^\star = k_\theta v_d = -\frac{m}{r}\frac{T_e}{eB}\kappa_n$ [black solid line in Fig. 5(a)]. It should be noted that the azimuthal number of the most unstable mode is higher than that observed in smaller devices, such as in Refs. 8 and 14, due to the larger plasma radius. As the mode number further increases, the instability growth rate decreases due to the effects of the ion Larmor radius, which are accounted for in the gyro-average operator and the polarization term.

For helium, the most unstable mode $m = 32$ is characterized by the highest instability growth rate $\omega_i = 4.616 \times 10^3$ s^{-1}, with a real frequency of 3.46×10^4 s^{-1}. We observe that the azimuthal number of the most unstable mode is greater than that obtained in the case of argon plasma.

For the second case with $B = 0.44$ T, an ITG is considered, resulting in a ratio $\eta = \frac{\kappa_T}{\kappa_n} = 5$ (Fig. 5). For argon, only the first three modes correspond to DW with positive real frequencies. Starting from $m = 4$, the negative real frequencies correspond to ITG instabilities that propagate in the direction opposite to electron diamagnetic velocity. In this case, the most unstable mode is $m = 16$, with a real frequency of -4.29×10^3 s^{-1}. It should be noted that both DW and ITG are unstable in this scenario, but ITG has higher instability growth rates.

For helium, only the first nine modes correspond to DW with positive real frequencies. Starting from $m = 10$, the negative real frequencies correspond to ITG instabilities that propagate in the direction opposite to the electron diamagnetic velocity. In this case, the most unstable mode is $m = 55$, with a real frequency of -1.32×10^4 s^{-1}. The most unstable mode in this case for a helium plasma is much higher than that obtained for ITG in the case of an argon plasma.

We, now, investigate the transition from collisional DW to ITG instability depending on the ITG, or more precisely, on the parameter $\kappa_T = \partial_r \ln T_i$.[33] If this parameter is zero, only DW occur. The
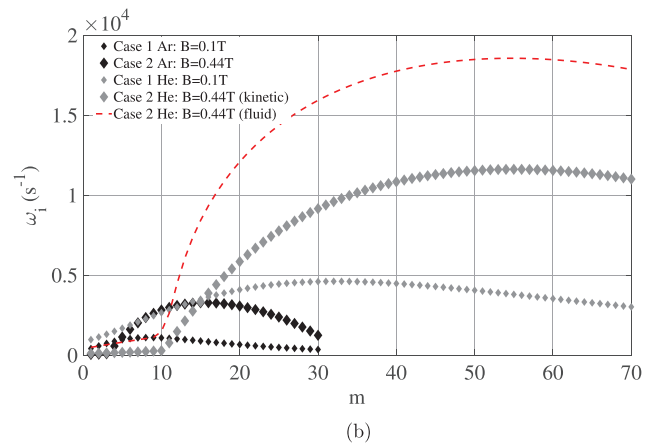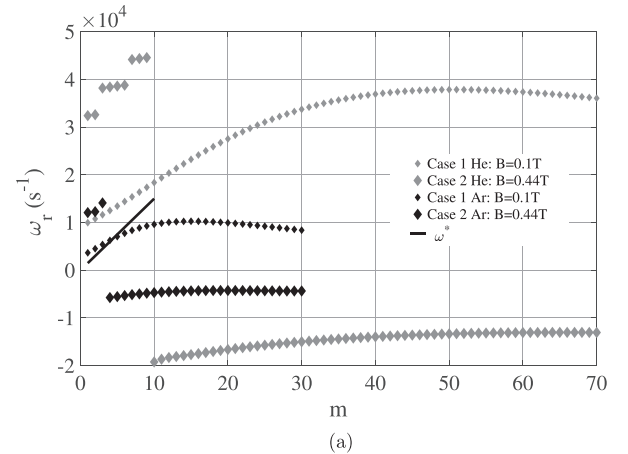

(a)

(b)

FIG. 5. Real frequency ω_r (a) and instability growth rate ω_i (b) plotted against the mode m. (a) Real frequency ω_r plotted against the mode m. For $B = 0.1$ T (first case), the most unstable mode for argon is $m = 8$ [see (b)], with $\omega_r = +8.873 \times 10^3$ s^{-1} corresponding to DW instability. The black solid line corresponds to the electron diamagnetic frequency $\omega^\star$ for argon plasma and in this first case. For helium, the most unstable mode is $m = 32$, with $\omega_r = +3.461 \times 10^4$ s^{-1} that corresponds to DW instability. For $B = 0.44$ T (second case with $\eta = 5$), the most unstable mode for argon is $m = 16$ [see (b)], with $\omega_r = -4.285 \times 10^3$ s^{-1} corresponding to ITG instability. For helium, the most unstable mode is $m = 55$, with $\omega_r = -1.316 \times 10^4$ s^{-1} that corresponds to ITG instability. (b) Instability growth rate ω_i plotted against the mode m. For $B = 0.1$ T (first case), the most unstable mode for argon is $m = 8$, with $\omega_i = 1.099 \times 10^3$ s^{-1}. For helium, the most unstable mode is $m = 32$, with $\omega_i = 4.616 \times 10^3$ s^{-1}. For $B = 0.44$ T (second case, kinetic model, with $\eta = 5$), the most unstable mode for argon is $m = 16$, with $\omega_i = 3.281 \times 10^3$ s^{-1}. For helium, the most unstable mode is $m = 55$, with $\omega_i = 1.162 \times 10^4$ s^{-1}. The second case, fluid model, red dotted line, will be discussed in Sec. VI.

parameter $\eta = \kappa_{T_i}/\kappa_n = \frac{1}{r}\partial_r T_i / \frac{1}{r}\partial_r n$ has to exceed a critical value to observe an ITG instability. This parameter can be increased either by flattening the density gradient or by increasing the ion-temperature gradient. Here, the increase in the ion-temperature gradient is chosen: we consider that ICRH in SPEKTRE will heat the plasma in the core resulting in an ITG. The parameter r_{T_i} will decrease as ICRH power increases, but will remain much greater than the ion Larmor radius. The bifurcation scenario between collisional DW and ITG with

different η in the magnetized plasma column is shown in Fig. 6. By increasing η, we observe bifurcations from DW to ITG as soon as $\eta = 2.6$. This can be seen by the change in the real frequency of the most unstable mode as a function of η [see Fig. 6(a)]. For $\eta \in [0.0 \ 2.6]$, the real frequencies of the most unstable modes are positive and correspond to DW; ω_r is almost equal to the electron diamagnetic pulsation ω^*, and the perturbation propagates in the electron diamagnetic drift direction as expected for DW. It should be noted that for one mode m, the frequency increases until the mode suddenly changes with a higher frequency. Once η exceeds 2.6, ITG instabilities become more unstable and correspond to negative real frequencies, propagating in the ion diamagnetic drift direction. The linear growth rate then continues to increase with η.
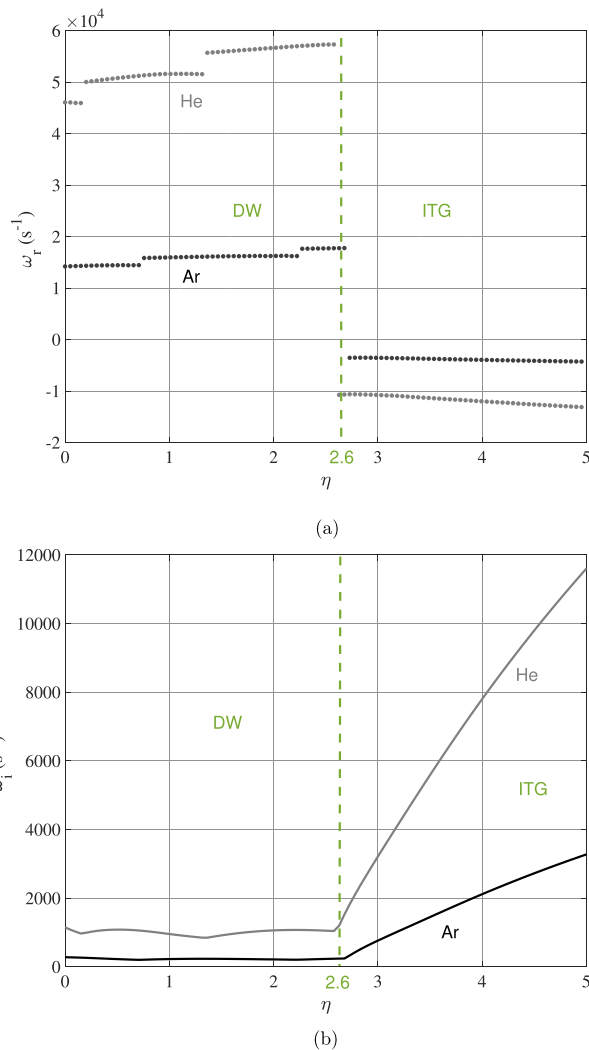
To conclude, we observe that in the SPEKTRE device, using an argon or an helium plasma, a transition between DW and ITG instabilities can be achieved through ion heating. The transition between these instabilities will be led by the ICRH system. The transition will appear at $\eta = 2.6$. In the case of $B = 0.44$ T and $\eta = 5$ for instance, modes around $m = 16$ should be observed for argon plasmas. For helium plasmas, modes of the order of $m = 55$ should be observed if the ratio $\eta = 5$ is maintained.

Furthermore, an important result to highlight is that the transition from DW to ITG occurs at the same value of $\eta = 2.6$ for both argon and helium plasmas. Since η is the ratio of the ion temperature profile to the density profile, the transition depends very little on the type of gas considered, but a slight difference can occur when the ion temperature decreases: for instance, for $T_{i_0} = 5$ eV, the transition occurs at $\eta = 2.73$ for argon, and $\eta = 2.83$ for helium.

Finally, we observed that the maximum growth rates for ITG (case 2) are achieved for nearly the same value of $k_\theta \rho_i$ for both argon and helium, just as the maximum growth rates for DW (case 1) correspond to nearly the same value of $k_\theta \rho_s$ for both gases.

VI. FLUID VS KINETIC RESULTS

In this section, we investigate the importance of using a kinetic model to accurately describe instabilities. We focus on the second case ($B = 0.44$ T), considering a helium plasma with $\eta = 5$. It should be noted that argon could have been chosen, as the results are very similar. We compare the results obtained from the kinetic model [Eq. (21)] with those from the fluid model [Eq. (22)].

The results are presented in Fig. 7. The ratio of kinetic vs fluid instability growth rates is plotted against T_i. The blue squares correspond to DW predicted by both the fluid and kinetic models. In this scenario (DW) and for this range of ion temperature, the instability growth rates and real frequencies predicted by the fluid and kinetic models are very close to each other. The black squares represent an ion temperature interval $[0.4, 0.6]$ eV for which the fluid model predicts ITG instabilities while the kinetic model predicts DW. The red squares correspond to ITG instabilities predicted by both the fluid and kinetic models. The fluid model overestimates the instability growth rate for ITG instabilities. Specifically, the kinetic instability growth rate is
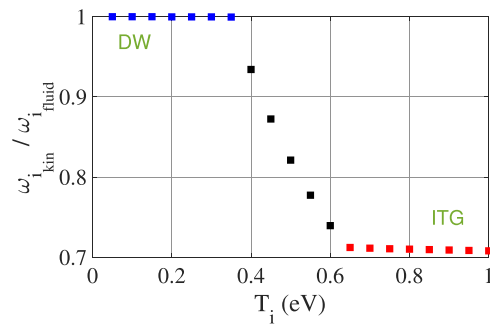
(a)

(b)

FIG. 6. Real frequency ω_r (6(a)) and instability growth rate ω_i (6(b)) plotted against $\eta = \kappa_T / \kappa_n$. The bifurcation from DW to ITG occurs at around $\eta = 2.6$. (a) Real frequency ω_r of the most unstable mode m plotted against η for $B = 0.44$ T (2nd case) for argon and helium. (b) Instability growth rate ω_i of the most unstable mode m plotted against η for $B = 0.44$ T (2nd case) for argon and helium.

FIG. 7. Ratio of kinetic vs fluid instability growth rates plotted against T_i. Plasma parameters: $\eta = 5$, $B = 0.44$ T, $T_e = 10$ eV, $m = 55$, using helium gas. Blue squares represent collisional DW predicted by both fluid and kinetic models. Black squares represent an ion temperature interval for which the fluid model predicts ITG instabilities while the kinetic model predicts DW. Red squares represent ITG predicted by both fluid and kinetic models. It appears that the fluid model overestimates the instability growth rate for ITG instabilities.

approximately 70% of the fluid instability growth rate for $T_i = 1$ eV, and this ratio decreases to about 60% for $T_i = 10$ eV. It should be noted that the real frequencies predicted by both fluid and kinetic models for are very similar.

To confirm this difference, we examine case 2 using helium gas with $\eta = 5$ and $T_i = 10$ eV. Figure 5(b) shows the instability growth rates predicted by both the kinetic and fluid (red dotted line) models plotted against m. The most unstable mode remains the same ($m = 55$), but the ratio of kinetic to fluid instability growth rates is 0.63, indicating that the fluid model overestimates the instability growth rates, even for DW in this case.

It is also noteworthy that similar results are obtained in the case of argon gas, and that the difference between the kinetic and fluid instability growth rates increases as η decreases.

VII. CONCLUSION

The model presented in this work is suitable for the numerical investigation of DW and ITG instabilities in cylindrical geometry. It serves as a useful and efficient tool for obtaining the linear kinetic ITG or DW instability growth rates and identifying the fastest growing modes that are likely to be observed in the large linear SPEKTRE device.

Furthermore, as anticipated, the ITG instability is highly dependent on the η parameter. It has been demonstrated that a transition between DW and ITG instabilities occurs around $\eta = 2.6$ for both argon and helium plasmas, at which point the ITG instability becomes dominant. Since η is the ratio of the ion temperature profile over the density profile, the transition depends very little on the gas considered, although the most unstable mode depends on the gas. It is noted that a small difference can occur when the ion temperature decreases. With the power deposition of Ion Cyclotron Resonance Heating (ICRH), this critical value of η should be attainable in the SPEKTRE device. ICRH in SPEKTRE will serve as an effective tool for investigating the DW-ITG transition.

Additionally, it has been shown that the kinetic model is necessary for accurately describing ITG instabilities under the plasma parameters expected in SPEKTRE, since the phase velocity of the ITG instabilities will be of the order of the ion thermal velocities. Although the real frequencies and the most unstable modes predicted by the fluid and kinetic models are very close to each other, the fluid model overestimates the instability growth rate by 60% to 70%. This discrepancy can significantly influence the turbulence level, as the quasi-linear theory predicts saturation levels proportional to the instability growth rates.

The density and temperature profiles shown in Fig. 2 enabled us to conduct this study. This choice was relatively arbitrary, pending the exact experimental profiles. However, even if the most unstable mode varies slightly depending on the profiles, the trends remain the same, as do the orders of magnitude of the obtained frequencies. This has been verified, for example, with a flat density profile. For ITG-type instabilities, in the case of helium, we, thus, obtain mode 50 as the most unstable mode (instead of mode 55), with a growth rate multiplied by 1.4 and a real frequency multiplied by 1.9. In the case of argon, the most unstable mode remains mode 16, with a growth rate multiplied by 1.6 and a real frequency multiplied by 1.75. The spatial and temporal characteristics of instability modes predicted by our study are important for the design of diagnostics that will equip the SPEKTRE machine, particularly concerning probe arrays.

The waves observed experimentally in MIRABELLE or COLUMBIA exhibit a fairly regular and nearly sinusoidal behavior. It has been demonstrated that it is reasonable to assume that these waves correspond to the fastest-growing modes of the linear analysis.[8,14] However, within the context of the SPEKTRE device, much higher modes are foreseen, and nonlinear interactions are expected to be strengthened, leading to more developed turbulence.

AUTHOR DECLARATIONS
Conflict of Interest

The authors have no conflicts to disclose.

Author Contributions

Etienne Gravier: Conceptualization (equal); Data curation (equal); Formal analysis (equal); Funding acquisition (equal); Investigation (equal); Methodology (equal); Software (equal); Supervision (equal); Validation (equal); Visualization (equal); Writing – original draft (equal); Writing – review & editing (equal). **Frederic Brochard:** Conceptualization (equal); Funding acquisition (equal); Validation (equal). **Maxime Lesur:** Conceptualization (equal); Formal analysis (equal); Validation (equal). **Jérôme Moritz:** Conceptualization (equal); Validation (equal). **Stephane Heuraux:** Conceptualization (equal); Formal analysis (equal); Validation (equal). **Damien Geneve:** Conceptualization (equal). **Timothé Rouyer:** Conceptualization (equal); Formal analysis (equal). **Daniele Del Sarto:** Conceptualization (equal); Validation (equal). **Eric Faudot:** Conceptualization (equal). **Alain Ghizzo:** Conceptualization (equal). **Nicolas Lemoine:** Conceptualization (equal). **Thierry Reveille:** Conceptualization (equal). **Guillaume Urbanczyk:** Conceptualization (equal).

DATA AVAILABILITY

The data that support the findings of this study are available from the corresponding author upon reasonable request.

REFERENCES

[1]F. Brochard, D. Geneve, S. Heuraux, V. Bobkov, D. Del Sarto, E. Faudot, A. Ghizzo, E. Gravier, N. Lemoine, M. Lesur, N. Louis, J. Moritz, T. Reveille, V. Rohde, U. Stroh, G. Urbanczyk, F. Volpe, and H. Zohm, in *49th EPS Conference on Plasma Physics*, P1.098, hal-04171543 (Bordeaux Congress Centre, 2023).
[2]H. W. Hendel, T. K. Chu, and P. A. Politzer, Phys. Fluids **11**, 2426 (1968).
[3]T. C. Simonen, T. K. Chu, and H. W. Hendel, Phys. Rev. Lett. **23**, 568 (1969).
[4]T. Klinger, A. Latten, A. Piel, G. Bonhomme, T. Pierre, and T. Dudok de Wit, Phys. Rev. Lett. **79**, 3913 (1997).
[5]E. Wallace, E. Thomas, A. Eadon, and J. Jackson, Rev. Sci. Instrum **75**, 5160 (2004).

[6]S. Aggarwal, Y. Camenen, A. Escarguel, and A. Poyé, J. Plasma Phys. **89**, 905890310 (2023).

[7]E. Gravier and E. Plaut, Phys. Plasmas **20**, 042105 (2013).

[8]E. Gravier, E. Plaut, X. Caron, and M. Jenny, Eur. Phys. J. D **67**, 7 (2013).

[9]E. Gravier, F. Brochard, G. Bonhomme, T. Pierre, and J. L. Briaçon, Phys. Plasmas **11**, 529 (2004).

[10]A. K. Sen, J. Chen, and M. Mauel, Phys. Rev. Lett. **66**, 429 (1991).

[11]F. Brochard, E. Gravier, and G. Bonhomme, Phys. Plasmas **12**, 062104 (2005).

[12]C. Schröder, O. Grulke, T. Klinger, and V. Naulin, Phys. Plasmas **11**, 4249 (2004).

[13]R. Scarmozzino, A. K. Sen, and G. A. Navratil, Phys. Rev. Lett. **57**, 1729 (1986).

[14]R. G. Greaves, J. Chen, and A. K. Sen, Plasma Phys. Control. Fusion **34**, 1253 (1992).

[15]W. Gekelman, H. Pfister, Z. Lucky, J. Bamber, and D. Leneman, Rev. Sci. Instrum. **62**, 2875 (1991).

[16]S. Oldenbürger, S. Inagaki, T. Kobayashi, H. Arakawa, N. Ohyama, K. Kawashima, Y. Tobimatsu, A. Fujisawa, K. Itoh, and S.-I. Itoh, Plasma Phys. Control. Fusion **54**, 055002 (2012).

[17]E. L. Shi, G. W. Hammett, T. Stoltzfus-Dueck, and A. Hakim, J. Plasma Phys. **83**, 905830304 (2017).

[18]B. N. Rogers and P. Ricci, Phys. Rev. Lett. **104**, 225002 (2010).

[19]B. J. Frei, J. Mencke, and P. Ricci, Phys. Plasmas **31**, 012301 (2024).

[20]P. Morel, E. Gravier, N. Besse, R. Klein, A. Ghizzo, P. Bertrand, X. Garbet, P. Ghendrih, V. Grandgirard, and Y. Sarazin, Phys. Plasmas **14**, 112109 (2007).

[21]I. Shesterikov, K. Crombe, A. Kostic, D. A. Sitnikov, M. Usoltceva, R. Ochoukov, S. Heuraux, J. Moritz, E. Faudot, F. Fischer, H. Faugel, H. Fünfgelder, G. Siegl, and J.-M. Noterdaeme, Rev. Sci. Instrum. **90**, 083506 (2019).

[22]S. Shinohara, Adv. Phys.: X **3**, 1420424 (2018).

[23]P. Baille, J.-S. Chang, A. Claude, R. M. Hobson, G. L. Ogram, and A. W. Yau, J. Phys. B: Atom. Mol. Phys. **14**, 1485 (1981).

[24]M. C. Kelley, *The Earth's Ionosphere*, 2nd ed. (Elsevier, 2009).

[25]S. A. Self, J. Plasma Phys. **4**, 693 (1970).

[26]R. F. Ellis and E. Marden-Marshall, Phys. Fluids **22**, 2137 (1979).

[27]R. F. Ellis, E. Marden-Marshall, and R. Majeski, Plasma Phys. **22**, 113 (1980).

[28]M. Dimits, G. Bateman, M. A. Beer, B. I. Cohen, W. Dorland, G. W. Hammet, C. Kim, J. E. Kinsey, M. Kotschenreuter, A. H. Kritz, L. L. Lao, J. Mandrekas, W. M. Nevins, S. E. Parker, A. J. Redd, D. E. Shumaker, R. Sydora, and J. Weiland, Phys. Plasmas **7**, 969 (2000).

[29]T. S. Hahm, Phys. Fluids **31**, 2670 (1988).

[30]F. F. Chen, Phys. Fluids **9**, 965 (1966).

[31]D. Mandal, M. Lesur, E. Gravier, J. N. Sama, A. Guillevic, Y. Sarazin, and X. Garbet, Plasma Phys. Control. Fusion **65**, 055001 (2023).

[32]V. G. Pryimak and T. Miyazaki, J. Comp. Phys. **142**, 370 (1998).

[33]J. W. Connor and H. R. Wilson, Plasma Phys. Control. Fusion **36**, 719 (1994).

05 January 2025 10:08:53